Biophysical Characterization of an Integrin-Targeted Lipopolyplex Gene Delivery Vector†

M. Firouz Mohd Mustapa,‡ Paul C. Bell,‡ Christopher A. Hurley,‡,¶ Alastair Nicol,§ Erwann Guénin,‡,+ Supti Sarkar,|| Michele J. Writer,⊥ Susie E. Barker,⊥ John B. Wong,‡ Michael A. Pilkington-Miksa,‡ Brigitte Papahadjopoulos-Sternberg,# Parviz Ayazi Shamlou,⊗ Helen C. Hailes,‡ Stephen L. Hart,⊥ Daniel Zicha,*,§ and Alethea B. Tabor*,‡

Department of Chemistry, Christopher Ingold Laboratories, University College London, 20 Gordon Street, London WC1H 0AJ, United Kingdom, Cancer Research U.K. London Research Institute, Lincoln's Inn Fields Laboratories, 44 Lincoln's Inn Fields, London WC2A 3PX, United Kingdom, Department of Biochemical Engineering, University College London, Torrington Place, London WC1E 7JE, United Kingdom, Nanoanalytical Laboratory, 3951 Sacramento Street, San Francisco, California 94118, and Wolfson Centre for Gene Therapy of Childhood Disease, Institute of Child Health, University College London, 30 Guilford Street, London WC1N 1EH, United Kingdom

Received May 24, 2007; Revised Manuscript Received August 8, 2007

ABSTRACT: Nonviral gene delivery vectors now show good therapeutic potential: however, detailed characterization of the composition and macromolecular organization of such particles remains a challenge. This paper describes experiments to elucidate the structure of a ternary, targeted, lipopolyplex synthetic vector, the LID complex. This consists of a lipid component, Lipofectin (L) (1:1 DOTMA:DOPE), plasmid DNA (D), and a dual-function, cationic peptide component (I) containing DNA condensation and integrin-targeting sequences. Fluorophore-labeled lipid, peptide, and DNA components were used to formulate the vector, and the stoichiometry of the particles was established by fluorescence correlation spectroscopy (FCS). The size of the complex was measured by FCS, and the sizes of LID, L, LD, and ID complexes were measured by dynamic light scattering (DLS). Fluorescence quenching experiments and freeze−fracture electron microscopy were then used to demonstrate the arrangement of the lipid, peptide, and DNA components within the complex. These experiments showed that the cationic portion of the peptide, I, interacts with the plasmid DNA, resulting in a tightly condensed DNA−peptide inner core; this is surrounded by a disordered lipid layer, from which the integrin-targeting sequence of the peptide partially protrudes.

Gene therapy is the delivery of exogenous genetic material (DNA/RNA) to a cell to correct a genetic defect or to express a specific protein. The concept is exceptionally powerful as the technique can be used to correct genetic disorders or treat diseases for which the pathophysiology is well understood. Although the concept has shown proof of principle, the discovery of a safe, viable vector for *in vivo* applications is ongoing. Viral vectors, particularly adenoviral and retroviral systems, are currently the vectors of choice for clinical use, as the transfection efficiency of viral vectors is good. However, viral vectors suffer several major disadvantages, such as insertional mutagenesis, restriction to dividing cells, and immunogenicity (*1*), and severe problems have been observed during clinical trials (*2*, *3*). Nonviral transfection methods, such as lipofection (*4*), electroporation (*5*), and nanoparticle delivery (*6*), have therefore recently received much attention.

The two major approaches to the preparation of synthetic vectors typically involve the condensation of polyanionic nucleic acids with polycationic polymers (polyplexes) such as polyethylenimine (PEI[1]), dendrimers, and peptides and/or with cationic lipids (lipoplexes) (*7*, *8*). Although such synthetic vectors have many advantages over viral vectors,

† This work was supported by grants from the BBSRC (to P.C.B. and E.G., 31/E11945; to M.F.M.M., BBS/B/03645) and the Cystic Fibrosis Trust (to M.J.W.) and by EPSRC studentships (to C.A.H., M.A.P.-M., S.S., and J.B.W.) and a MRC studentship (to S.E.B.).

* Author to whom correspondence should be addressed [(A.B.T.) telephone 020 7679 4695, fax 020 7679 7463, e-mail a.b.tabor@ucl.ac.uk; (D.Z.) telephone 020 7269 3563, e-mail daniel.zicha@cancer.org.uk].

‡ Department of Chemistry, University College London.

¶ Present address: Argenta Discovery Ltd., 7-9 Spire Green Centre, Flex Meadow, Harlow, CM19 5TR, U.K.

§ Cancer Research U.K. London Research Institute.

+ Present address: Chimie Structurale et Spectroscopie Biomoléculaire, UMR CNRS 7033, (porte 315), 74 rue Marcel Cachin, 93017 Bobigny Cedex, France.

|| Department of Biochemical Engineering, University College London.

⊥ Institute of Child Health, University College London.

Nanoanalytical Laboratory.

⊗ Present address: Process Engineering Center, Eli Lilly and Co., Lilly Corporate Center, DC 3127, Indianapolis, IN 46285.

[1] Abbreviations: AFM, atomic force microscopy; β-BODIPY 500/510 C_{12}-HPC, 2-(4,4-difluoro-5-methyl-4-bora-3a,4a-diaza-*s*-indacene-3-dodecanoyl)-1-hexadecanoyl-*sn*-glycero-3-phosphocholine; β-BODIPY 581/591 C_5-HPC, 2-(4,4-difluoro-5-(4-phenyl-1,3-butadienyl)-4-bora-3a,4a-diaza-*s*-indacene-3-pentanoyl)-1-hexadecanoyl-*sn*-glycero-3-phosphocholine; Dde, 1-(4,4-dimethyl-2,6-dioxocyclohex-1-ylidene)-ethyl; DLS, dynamic light scattering; DOPE, dioleoylphosphatidylethanolamine; DOTMA, *N*-[1-(2,3-dioleyloxy)propyl]-*N*,*N*,*N*-trimethylammonium chloride; FCS, fluorescence correlation spectroscopy; Mca, *N*-(fluoren-9-ylmethoxycarbonyl)-*N*-[(7-methoxycoumarin-4-yl)acetyl]; PEI, polyethylenimine.

10.1021/bi701014y CCC: $37.00
Published on Web 10/13/2007

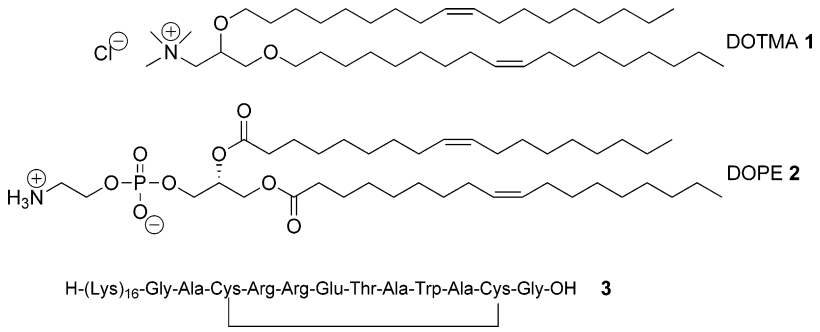

FIGURE 1: Components of LID vector.

including lower immunogenicity, ease of large-scale preparation, and unlimited packaging capacity, poor gene transfer efficiencies have to date precluded their use. Many attempts have been made to improve the efficacy and selectivity of synthetic vectors by imitating the biological mechanisms utilized by viruses for gene delivery (*9*). In particular, synthetic vectors have been targeted to specific cell-surface receptors, in order to use receptor-mediated endocytosis pathways to transport the vector into the cell and to mediate subsequent gene delivery steps (*10*). Such targeting moieties include peptides, polysaccharides, and antibodies, which may also confer cell specificity upon the synthetic vector.

Ternary synthetic vectors, combining the advantages of polyplexes and lipoplexes, have recently been described by several groups including Hart et al. (*11*). These targeted, self-assembling lipid/peptide (lipopolyplex) vector complexes (LID) consist of a lipid component, Lipofectin (L) [the cationic lipid DOTMA (**1**) with a co-lipid DOPE (**2**) in a 1:1 ratio], plasmid DNA (D), and a dual-function, cationic peptide component (I) (**3**) containing DNA condensation and integrin-targeting sequences (Figure 1). LID systems were shown to display high transfection efficiency and low toxicity *in vitro* and *in vivo*, to transfect nondividing cells efficiently, and were well tolerated with low immunogenicity *in vivo* (*11*−*14*).

A complete picture of the structure and macromolecular organization of synthetic gene delivery vectors is clearly crucial to understand their mode of action and to optimize gene transfer. Lipoplex-based vectors have previously been characterized by various physicochemical methods including electron microscopy and AFM, and clearer pictures of the morphologies of the particles and the effects on transfection properties are emerging (*8*, *15*−*20*). However, characterization studies on polyplex vectors and on more complex ternary systems (*21*) remain rare.

To understand the mechanism of action of the LID complexes, and with the aim of further optimizing both the gene transfer and stability properties of this family of vectors, we have undertaken a detailed investigation of the structure and stoichiometry of the LID particles. It was clear from the original study (*11*) that the LID complex undergoes integrin-mediated endocytosis and that the integrin recognition sequence must therefore be presented to receptors on the cell surface. However, Lipofectin also plays a key role, in the original study increasing luciferase expression by >100-fold relative to complexes formed from the peptide and DNA components alone. In the present study, we sought to answer several key questions about the LID complexes. It was not known whether both of the lipid components were, in fact, incorporated in the LID particle in the stoichiometry and ratio in which they were mixed, nor whether all of the peptide had been incorporated—at the 4:1 charge ratio used in the original study, this would lead to a particle with a very high zeta potential. The spatial arrangement of the three components was also not known, in particular whether the lipid formed a monolayer, an ordered bilayer, or a multilamellar structure, and whether the lipid was on the exterior of the particle or incorporated within the condensed peptide−DNA complex. It was therefore of vital importance to establish the stoichiometry of both peptide and lipid components contained in the LID complex and the macromolecular organization of the particles.

Few techniques are available for the detailed study of the composition and macromolecular structure of self-assembling complexes such as micelles and liposomes. Fluorescence correlation spectroscopy (FCS), a technique in which the fluorescence intensity fluctuations of a small volume containing fluorescent particles is correlated to the underlying properties of the particles that give rise to such fluctuations, appeared to be a powerful method for examining such systems. FCS has recently been used to examine several biological processes, both *in vitro* and *in vivo*, particularly binding equilibria and kinetics, protein dimerization, and membrane dynamics (*22*−*24*). Of particular relevance to this study was the use of FCS to measure the number of molecules in micelles and the size of the micelles (*25*−*27*) and to examine the interactions between oligonucleotides and cationic peptides or polymers (*28*, *29*). In this paper we have used FCS to determine the number of integrin-binding peptides **3** and of DOTMA and DOPE molecules incorporated within the LID lipopolyplex, and we have also determined the size of the LID complexes.

On the basis of the optimum method of formulation of the LID particles, and their biological properties, several models for the relative arrangements of peptide, lipid, and plasmid DNA within the particles could be envisaged. To elucidate the macromolecular organization of the complexes, we have carried out a series of fluorescence quenching experiments, designed to indicate which component(s) of the vector are buried within the complex and which are free to interact with the target cell. We have also used dynamic light scattering (DLS) as an alternate method of determining the size of the LID particles and have determined the size of the Lipofectin liposomes and a peptide−DNA complex to further elucidate the correct spatial arrangement.

Finally, electron microscopy has recently emerged as a powerful technique for studying lipoplex-based gene delivery, enabling the morphology of particles of various com-

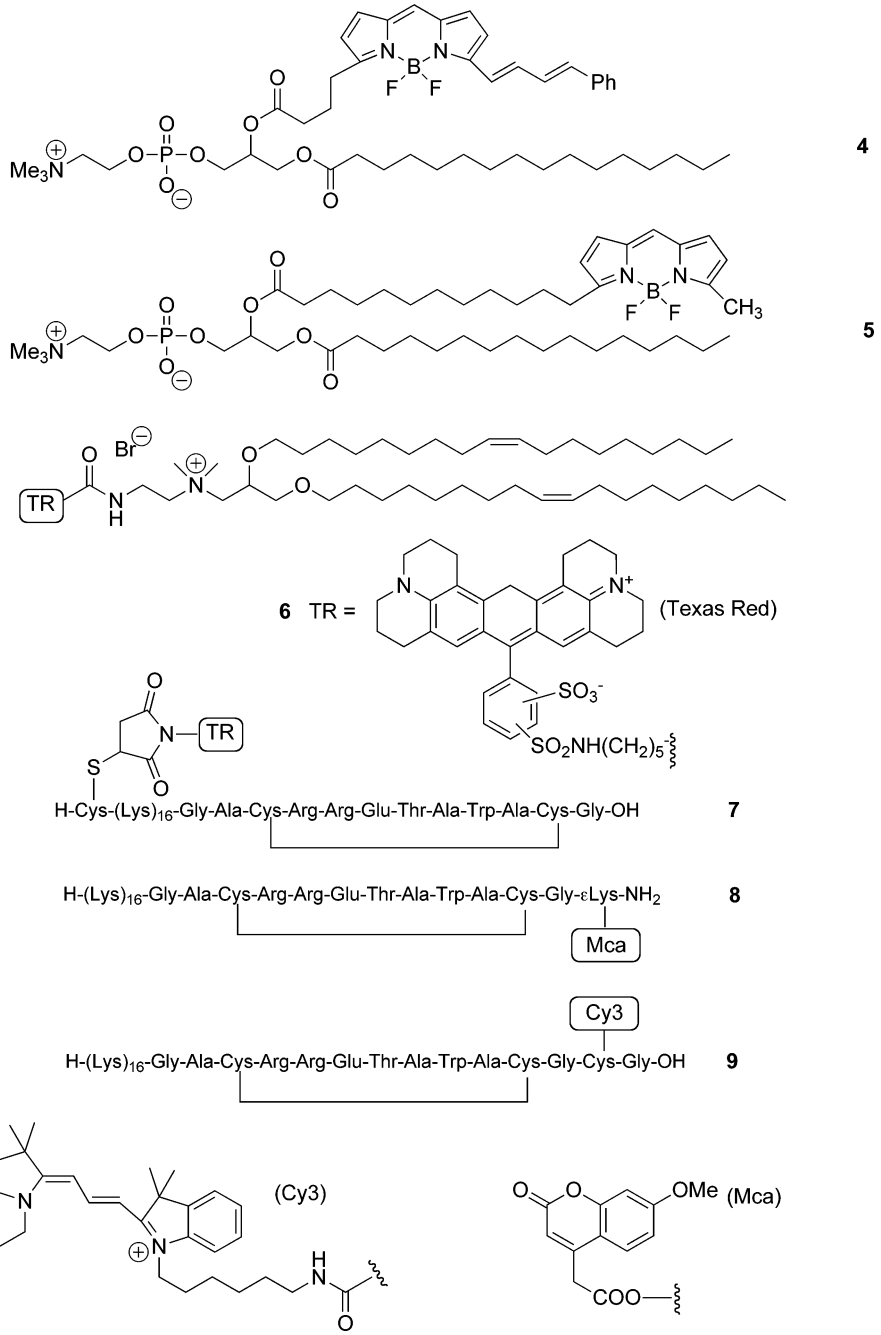

FIGURE 2: Fluorophore-labeled peptides and lipids.

positions and charge ratios to be studied (*15*, *30*−*42*), and we have therefore carried out freeze−fracture electron microscopy on the LID particles.

Combining the details of the LID morphology from these EM studies with the FCS, DLS, and fluorescence quenching experiments has afforded us a clear picture of the macromolecular organization of these unique, self-assembling gene delivery vectors.

MATERIALS AND METHODS

Fluorescently Labeled Materials. For the FCS and fluorescence quenching experiments, it was imperative to use analogues of the lipids **1** and **2** and of the peptide **3**, which were regioselectively fluorescently labeled in a structurally conservative manner (Figure 2). DOPE analogues **4** (*β*-BODIPY581/591 C_5-HPC) and **5** (*β*-BODIPY500/510 C_{12}-HPC), both labeled with BODIPY within the fatty acid chain, were purchased from Invitrogen. DOTMA analogues specifically labeled at the headgroup with Texas Red (**6**) were synthesized using a modification of a method developed in our laboratories (*43*). Labeled peptides **7**, **8**, and **9** were also prepared. These were synthesized using standard solid-phase methods, with the Cys residues (**7** and **9**) that would ultimately bear the label protected with Acm (*44*). Cleavage of the remaining protecting groups and oxidation to form the required disulfide linkage was followed by Acm deprotection and derivatization with Texas Red maleimide (for **7**, purchased from Invitrogen) or Cy3 iodoacetamide [for **9** (*45*)]. For **8**, the Mca label was attached onto the peptide at the α-position of the Lys residue at the beginning of the peptide synthesis immediately after Fmoc deprotection. Subsequent amino acids were coupled following removal of

the Dde group from the ϵ-amine of the Lys residue (*46*). Peptides were isolated as their TFA salts after HPLC purification, and this has been taken into account when the peptides were weighed for stock solution preparation. Complete details of the synthesis of the labeled peptides and lipid will be reported elsewhere. Cy5-labeled plasmid DNA pCILuc was prepared using a Mirus Cy5 plasmid labeling kit (Mirus LabelIT, Panvera, CA) according to the manufacturer's instructions.

Complex Formation for FCS. The LID complexes were prepared following the method originally described in Hart et al. (*11*). For the LID complexes containing labeled peptide, Lipofectin was first prepared by mixing chloroform solutions of equal ratios of DOTMA/DOPE by weight and drying to a film under high vacuum for 24 h. This film was hydrated in Milli-Q water for 24 h and sonicated for 5 min to give a 0.05 mg/mL solution.

The complexes were then formulated, incorporating different percentages of fluorescent label, at different peptide/DNA charge ratios, as follows. Lipofectin (15 mL) was added to a solution (80 μL of 0.05 mg/mL for the 4:1 ratio and 80 μL of 0.0214 mg/mL for the 1.5:1 ratio, taking into account the TFA counterions associated with each peptide) of peptide **3** containing 0.1, 0.5, 1, 5, 10, and 20% of Cy3-labeled peptide **9** and left to mature for 5 min. Plasmid DNA pGL2 (*11*) (100 μL, 0.01 mg/mL) was added and the complex matured at 4 °C overnight in the dark. The same method was followed with LID complexes containing increasing percentages of Texas Red-labeled peptide 7 (4:1 overall peptide/DNA charge ratio). The resulting complexes had a Lipofectin/peptide/DNA weight ratio of 0.75:4:1 (for the 4:1 charge ratio) and 0.75:1:1 (for the 1.5:1 charge ratio).

For the LID complexes containing labeled lipid, the liposomes were first prepared at labeled lipid concentrations of 0.1, 0.5, 1, 5, and 10% of the total lipid concentration with either **4** or **6**. These labeled liposomes were then used to prepare LID complexes at 4:1 peptide (N)/DNA (P) charge ratios, as described above. The resulting complexes had a Lipofectin/peptide/DNA weight ratio of 0.75:4:1.

The transfection of the LID complex (4:1 charge ratio) incorporating 10% Cy3-labeled peptide **9** was checked via a luciferase assay, carried out as in ref *11*. These experiments indicated a very slight attenuation of transfection (data not shown) possibly arising from a steric clash between the Cy3 label and the cell surface integrins.

FCS Experiments. Measurements were performed on a Confocor fluorescence correlation spectrometer (Carl Zeiss Jena GmbH) using a HeNe λ 543 nm laser. Samples were measured in a 96 well plate with a sample volume of 195 μL. Prior to each set of readings, the machine was first calibrated using a stock solution of Texas Red diluted to give a photon count rate of around 70 kHz and the structure parameter determined. The diffusion time of a stock solution of either the labeled lipid (**4** or **6**) or the labeled peptide (**7** or **9**), as appropriate to the experiment, was then measured, and the data were analyzed as described below. In each case, the data for the fluorophore-labeled lipid or peptide fit perfectly to a one-component model, indicating that in all cases no free dye was present in the solutions. (The purity of the labeled components was also confirmed by analytical HPLC.) From these measurements the structure parameter for the fluorophore-labeled lipid or peptide was calculated. The diffusion times of the various fluorescent LID complex samples, described above, were then measured. The data were analyzed as described below, with the structure parameter for the individual fluorophore-labeled lipid or peptide, previously calculated, being used as one component in the two-component analysis of the labeled LID complexes.

FCS Theory. The theory of fluorescence correlation spectroscopy was defined by Madge et al. (*47*, *48*) and is a technique that measures fluctuations in fluorescence over time to obtain information on dynamic molecular events over a microsecond−second time scale. Here we give a brief introduction to the technique; more detailed descriptions of the theory and applications can be found elsewhere (*22*, *23*, *49*). The time correlations of thermodynamic concentration fluctuations produced by FCS can be interpreted to give kinetic data on chemical reactions, binding constants for various host−guest interactions, and information on diffusion behavior of molecules or particles and hydrodynamic particle radii. To analyze the time course of fluctuations of the fluorescence $F(t)$ with respect to the average fluorescence F, the autocorrelation function is given (*50*) by

$$G(\tau) = \frac{\langle F(0)F(\tau)\rangle}{\langle F(\tau)\rangle^2} \tag{1}$$

These fluctuations are either derived from changes in the number of fluorescent particles in the focal volume or changes in the fluorescence yield of the particles. In our experiments the fluorophores were excited with a laser possessing a Gaussian beam profile, and therefore the focal volume can be approximated by a Gaussian distribution in the three Cartesian coordinate axes. The true probe volume is further defined as a Gaussian laser beam (GLB) profile and a pinhole that spatially filters the emitted fluorescence. From this it is possible to derive a term describing the focal volume, a structure parameter SP, where ω_2 corresponds to half the length of the confocal volume and ω_1 is the width.

$$\mathrm{SP} = \frac{\omega_2}{\omega_1} \tag{2}$$

In theory this should remain constant; however, variations in the calibration of the machine lead to small variations in the size of the focus and the pinhole and variations in SP. A single particulate species leads to the autocorrelation function to be described as

$$G(\tau) = \frac{\gamma}{N}\left(1 + \frac{\tau}{\tau_{\mathrm{diff}}}\right)^{-1}\left(1 + \frac{\tau}{\mathrm{SP}^2\tau_{\mathrm{diff}}}\right)^{-1/2} + G_\infty \tag{3}$$

where τ_{diff} is the diffusion time, γ is a correction factor, N is the mean number of fluorescent particles diffusing through the detection volume, and G_∞ is assumed to be 1 (G at $\tau \rightarrow \infty$). For a multicomponent system (R components), however, eq 3 becomes

$$G(\tau) = \frac{\sum_{i=1}^{\mathrm{R}} \alpha_i^2\langle N_i\rangle g_{3di}(\tau)}{[\sum_{i=1}^{\mathrm{R}} \alpha_i\langle N_i\rangle]^2} + G_\infty \tag{4}$$

where

$$g_{3di} = \left(1 + \frac{\tau}{\tau_{\text{diff}}}\right)^{-1}\left(1 + \frac{\tau}{\text{SP}^2\tau_{\text{diff}}}\right)^{-1/2}$$

FCS Data Analysis. The analysis of data derived from the lipopolyplex measurements was complicated by the heterogeneity of the LID formulation. The LID complexes were prepared following the method previously described (*11*), in order to study the exact formulation used in previous transfection experiments. However, this method of formulating this ternary mixture results in particles that were to some degree polydisperse in size, and the presence of a small number of large particles in solution leads to erroneous readings in the FCS experiments, due to large spikes in the observed fluorescence fluctuations. It was therefore necessary to identify and discard these readings in the course of the data analysis. The lipid data were processed using FCS+plus (Evotec Biosystems GmbH), with data containing large numbers of spikes eliminated by inspection.

The peptide data were fitted to a two-component function in Mathematica. The hardware autocorrelated data were analyzed initially on intensity for large spikes before treatment in Mathematica. After fitting, erroneous readings were discarded when they fell outside the following values for three key parameters: estimated variance < 0.0005; 0 < τ_{triplet} < 0.015; 25% > fraction of triplet > 0, after examination of their distribution with scatter plots and histograms. The mean values of τ and min and max values were then calculated according to the methods of Wohland et al. (*50*).

From the measured diffusion times we determined the hydrodynamic radii of the particles to compare the observed light scattering data and microscopy information.

Using free Texas Red dye we can derive ω_1 (the width of the confocal volume) from eq 5 as the diffusion coefficient is known.

$$\omega_1 = \sqrt{4D\tau_{\text{diff}}} \tag{5}$$

The diffusion coefficient of the particle was determined after rearranging eq 5 to yield

$$D = \frac{{\omega_1}^2}{4\tau_{\text{diff}}} \tag{6}$$

Utilizing the Stokes−Einstein equation, where k is the Boltzman constant, T is temperature, and η is the viscosity, we can therefore derive the radii of the particles.

$$r = \frac{kT}{6\pi\eta D} \tag{7}$$

Dynamic Light Scattering. In DLS a monochromatic laser beam is employed to probe a small volume of diffusing particles in a dilute colloidal suspension. As the particles undergo Brownian motion, the temporal fluctuation of the intensity of the scattered light is detected and analyzed using a correlator that yields, in real time, the autocorrelation function. This function is analyzed according to the method of cumulants, which gives a statistically determined *z*-average diameter and a population distribution of the complexes. The first cumulant is directly related to the effective translational diffusion coefficient from which the hydrodynamic diameter of the complex is obtained through the Stokes−Einstein relationship (*51*, *52*).

DLS measurements were performed using a Malvern Zetasizer 3000 instrument (Malvern Instruments Ltd., U.K.) operating at a wavelength of 633 nm and a power output of 5 mW. All experiments were conducted at a constant temperature of 25 °C and a scattering angle of 90°, and spectra were collected every 180 s for at least 30 min. For broad, irregularly shaped distributions, where the method of cumulants was inappropriate, the CONTIN "constrained regularization" program (*53*, *54*) was used for data analysis.

Freeze−Fracture Electron Microscopy (EM). For freeze−fracture EM the samples were quenched using a sandwich technique and liquid nitrogen-cooled propane. When this technique is used, a cooling rate of 10000 K/s is reached, avoiding ice crystal formation and artifacts possibly caused by the cryofixation process. The cryofixed samples were stored in liquid nitrogen for <2 h before processing. The fracturing process was carried out in JEOL JED-9000 freeze-etching equipment, and the exposed fracture planes were shadowed with Pt for 30 s in an angle of 25−35° and with carbon for 35 s (2 kV/ 60−70 mA, 1×10^{-5} Torr). The replicas produced this way were cleaned with concentrated, fuming HNO_3 for 24 h followed by repeating agitation with fresh chloroform/methanol (1:1 by vol) at least five times. The replicas cleaned this way were examined with a JEOL 100 CX electron microscope.

Five samples were examined by freeze−fracture EM: Lipofectin in water, alone (L); a lipoplex complex of Lipofectin/plasmid DNA (LD); a polyplex complex of peptide and plasmid DNA ($K_{16}D$); the LID complex itself at a 1.5:1 charge ratio; and an $LK_{16}D$ complex (where K_{16} is a truncated version of peptide **3** containing only Lys_{16}).

Fluorescence Quenching. Collisional quenching of fluorescence is described by the Stern−Volmer equation

$$\frac{F_0}{F} = 1 + k_q\tau_0[Q] \tag{8}$$

where F_0 and F are the fluorescence intensities in the absence and presence of quencher Q, respectively, k_q is the bimolecular quenching constant, and τ_0 is the lifetime of the fluorophore in the absence of quencher. For species in which a single population of fluorophores is present, all equally accessible to the quenching agent, a plot of F_0/F against [Q] (a Stern−Volmer plot) should therefore be linear, with a slope of $k_q\tau_0$ and an intercept of 1 on the *y*-axis (*55*).

Quenching experiments were then carried out with a series of LID complexes, bearing various labels on different components, as follows. All experiments were carried out using a FluoroMax-3 fluorometer with a xenon arc-lamp and DataMax 2.2 software, with the excitation and emission slit widths quoted (in nanometers) following corresponding wavelengths, and each solution was prepared using doubly distilled water adjusted to pH 7.2 with NaOH solution (2 M).

Complex Formation for Fluorescence Quenching Experiments. The LID complexes were prepared by adding the peptide solution (17.1 μL from 30 μM, 0.1 mg/mL stock solutions) to the liposome component (0.75 μL from 1 mg/

mL stock solutions). To the resulting mixture was added the DNA solution (pCI-Luciferase, 100 μL from 10 μg/mL stock solutions), topped with doubly distilled water (23.15 μL; total solution of 141 μL, left at room temperature to reach equilibrium for 1 h) to yield a resulting peptide concentration of 3.64 μM, a lipid/peptide/DNA weight ratio of 0.75:1:1, and a peptide/DNA charge ratio of 1.5:1.

A series of control fluorescence quenching experiments were also carried out using individual components of peptides and plasmid DNA, with each experiment using solutions prepared at the same concentration as specified in the corresponding LID complexes. The control experiments for the lipids were carried out in the same way in terms of total lipid concentrations, but with only 10% labeled solutions instead. The fluorescence was quenched by titration with an acrylamide solution (2.0 M, 1 μL additions totaling 9 μL, final volume of 150 μL) to the mixture.

*Mca-Labeled Peptide **8** Control.* A solution of Mca-labeled peptide **8** (17.1 μL from a 30 μM stock solution, diluted with doubly distilled water to 141 μL) was prepared. To this solution was added the acrylamide solution, and the change in emitted fluorescence at fixed wavelength [392 nm (4 nm), fluorescence maxima for Mca, excitation at 340 nm (4 nm)] measured after a 10 min equilibrium time was observed.

*Unlabeled Peptide **3** Control.* A solution of unlabeled peptide **3** (17.1 μL from a 30 μM stock solution, diluted with doubly distilled water to 141 μL) was prepared. To this solution was added the acrylamide solution, and the change in emitted fluorescence at fixed wavelength [356 nm (8 nm), fluorescence maxima for Trp residue, excitation at 295 nm (8 nm)] measured after a 10 min equilibrium time was observed.

*BODIPY-Labeled DOPE **5** Control.* Liposomes of lipids DOTMA and **5** (0.1 mg each) were prepared by initially dissolving in chloroform (20 μL, 10 mg/mL total lipid concentration) and then drying to a film under high vacuum for 24 h. This film was hydrated with doubly distilled water (200 μL) at 4 °C for 24 h, heated to 40 °C, and sonicated for 5 min. To 20 μL of this 1 mg/mL liposome solution was added 180 μL of Lipofectin solution, at the same concentration and prepared in the same way, left to equilibrate at 4 °C for 24 h, to yield 10% BODIPY-labeled Lipofectin. To part of this solution (0.75 μL, diluted with doubly distilled water to 141 μL) was added the acrylamide solution, and the change in emitted fluorescence at fixed wavelength [517 nm (7 nm), fluorescence maxima for BODIPY, excitation at 495 nm (7 nm)] measured after a 10 min equilibrium time was observed.

Cy5-Labeled Plasmid DNA Control. A solution of Cy5-labeled pCI-Luciferase (100 μL from a 10 μg/mL stock solution, diluted with doubly distilled water to 141 μL) was prepared. To this solution was added the acrylamide solution, and the change in emitted fluorescence at fixed wavelength [663 nm (6 nm), fluorescence maxima for Cy5, excitation at 649 nm (6 nm)] measured after a 10 min equilibrium time was observed.

For all of the above quenching experiments the data were plotted as Stern−Volmer plots.

Quenching of the Peptide Component. (a) LID. Unlabeled peptide **3**, Lipofectin, and pCI-Luciferase were used to prepare complexes at a 1.5:1 peptide/DNA charge ratio, as described above. To this solution (141 μL) was added the acrylamide solution, and the change in emitted fluorescence at fixed wavelength [354 nm (8 nm), fluorescence maxima for Trp residue, excitation at 295 nm (8 nm)] measured after a 10 min equilibrium time was observed.

*(b) LI*D.* Mca-labeled peptide **8**, Lipofectin, and pCI-Luciferase were used to prepare complexes at a 1.5:1 peptide/DNA charge ratio, as described above, resulting in a 100% labeled peptide complex. To this solution (141 μL) was added the acrylamide solution, and the change in emitted fluorescence at fixed wavelength [391 nm (5 nm), fluorescence maxima for Mca, excitation at 340 nm (5 nm)] measured after a 10 min equilibrium time was observed.

For all of the above quenching experiments the data were plotted as Stern−Volmer plots.

*Quenching of the Lipid Components. L*ID (DOPE).* BODIPY-labeled Lipofectin **5** (10% labeled, taken from the stock solution for the control experiment), peptide **3**, and pCI-Luciferase were used to prepare complexes at a 1.5:1 peptide/DNA charge ratio as described above. To this solution (141 μL) was added the acrylamide solution, and the change in emitted fluorescence at fixed wavelength [517 nm (6 nm), fluorescence maxima for BODIPY, excitation at 495 nm (6 nm)] measured after a 10 min equilibrium time was observed.

Quenching of the DNA Component. LID.* Peptide **3**, Lipofectin, and Cy5-labeled pCI-Luciferase were used to prepare complexes at a 1.5:1 peptide/DNA charge ratio as described above. To this solution (141 μL) was added the acrylamide solution, and the change in emitted fluorescence at fixed wavelength [670 nm (7 nm), slight shift in the fluorescence maxima for Cy5, excitation at 649 nm (7 nm)] measured after a 10 min equilibrium time was observed.

For all of the above quenching experiments the data were plotted as Stern−Volmer plots.

RESULTS

Stoichiometry of the LID Complexes. FCS differentiates well between species that have diffusion times, τ, which differ by an order of magnitude. As there is a considerable difference in size, and thus in τ, between the free lipid and the LID complex, and also between the free peptide and the LID complex, this makes the technique ideal for determining the extent to which each of the individual components is incorporated in the complexes. FCS measurements were first used to determine the percentage of each lipid incorporated in the LID particle. To study the incorporation of DOPE, a series of Lipofectin liposomes containing labeled lipid **4** were prepared at labeled lipid concentrations of 0.1, 0.5, 1, 5, and 10% of the total lipid concentration and used to formulate equivalently labeled LID particles. Lipid **4** alone, in the absence of other vector components, had a diffusion time of 0.123 ms. The LID data were most appropriately fitted by a two-component model, with component I being the free lipid and component II the LID complex. Fixing the diffusion time of component I to that obtained for the free lipid **4** generates a range of diffusion times of 4.32−6.53 ms for component II. The similarity of the diffusion times for component II indicates that the particle sizes across the concentration range are comparable and that similar complexes are forming at all labeled lipid concentrations studied. The percentage of component II detected over the various concentrations of

Table 1: Diffusion Times and Percentage of Species for Free Lipid **4** and Labeled L*ID Complex

	component I (BODIPY-DOPE **4**)	component II	
% labeled lipid **4**	diff time 0.123 ms, I (%)	diff time II (ms)	II (%)
0.1	1.1	4.81	98.9
0.5	1.0	4.80	99.0
1.0	1.2	4.32	98.8
5.0	0.6	4.86	99.4
10.0	4.3	6.53	95.7

Table 2: Diffusion Times and Percentage of Species for Free Lipid **6** and Labeled L*ID Complex

	component I (TxRed-DOTMA **6**)	component II	
% labeled lipid **6**	diff time 0.078 ms I (%)	diff time II (ms)	II (%)
0.1	9.0	3.89	91.0
0.5	13.5	3.92	86.5
1.0	9.5	3.79	90.5
10.0	7.5	5.12	92.5

labeled lipid suggested that high levels of labeled lipid incorporation occurred, consistently at levels of >95% (Table 1). This indicates that for the DOPE component of LID, 95% of the lipid added is incorporated.

Similar experiments were carried out using Lipofectin liposomes containing the DOTMA analogue, labeled lipid **6**, prepared at labeled lipid concentrations of 0.1, 0.5, 1, and 10% of the total lipid concentration, and used to formulate equivalently labeled LID particles. Free labeled **6** had a diffusion time of 0.078 ms. The LID data were also most appropriately fitted by a two-component model, with component I being the free lipid and component II the LID complex, and diffusion times for component II were found to be in the range of 3.79−5.12 ms. This compares favorably with the particles incorporating **4**, suggesting that the particle sizes in both studies are similar. Again, high levels of cationic lipid incorporation (86.5−92.5%) were observed (Table 2). The percentage incorporation of **6** is slightly lower than that observed for **4**; this could be due to the relative locations of the fluorophore within the lipid. For the headgroup-labeled DOTMA analogue **6**, unfavorable steric interactions between lipids, or between lipid and DNA, could influence the levels incorporated.

FCS measurements were then used to determine the percentage of the targeting peptide incorporated in the LID particle. As with the lipids, a series of labeled LID particles containing unlabeled Lipofectin, unlabeled peptide **3**, and labeled peptide **9**, were formulated at labeled peptide concentrations of 1, 5, and 10% of the total peptide concentration, and at a 4:1 peptide/DNA charge ratio, as originally described (*11*). Peptide **9** alone, in the absence of other vector components, had a diffusion time of 0.24 ms [standard error (SE) = 0.005]. The LID data were again fitted by a two-component model, with component I being the free peptide and component II the LID complex. Fixing the diffusion time of component I to that obtained for the free peptide **9** (0.24 ms) generates a range of diffusion times of 3.48−3.56 ms for component II. In these experiments, however, a far higher proportion of the labeled peptide,

Table 3: Diffusion Times and Percentage of Species for Free Peptide **9** and Labeled LI*D Complex, Formulated at a 4:1 Charge Ratio

	component I (peptide **9**)		component II			
% labeled peptide **9**	diff time 0.24 ms I (%)	SE	diff time II (ms)	SE	II (%)	no. of measurements
1.0	22.7	0.6	3.48	0.13	77.3	68
5.0	33.5	1.8	3.56	0.15	66.5	30
10.0	24.2	20.5	3.54	0.18	74.8	32

component I, was detected (Table 3), with a mean fraction of 26.8% (SE = 1.5%) of the total fluorescent particles. This indicates that, at this 4:1 peptide/DNA ratio, only about 70% of the peptide is incorporated in the resulting LID particles (Figure 3a). We therefore formulated a series of labeled LID particles containing unlabeled Lipofectin, unlabeled peptide **3**, and labeled peptide **9**, at labeled peptide concentrations of 0.1, 0.5, 1, 5, 10, and 20% of the total peptide concentration, at a 1.5:1 peptide/DNA charge ratio, and repeated the FCS measurements. In this case, fitting the data to a two-component model generates a range of diffusion times of 2.21−3.98 ms for component II (Table 4). In this case a mean fraction of only 16.7% (SE = 0.8%) of the labeled peptide alone (component I) was detected, indicating that approximately 85% of the peptide was incorporated in the LID particles at this charge ratio (Table 4 and Figure 3b). Again, the consistency of the diffusion times and percentage peptide incorporation indicate that similar complexes are forming at all labeled peptide concentrations studied and that the presence of the fluorophore at the integrin-recognition portion of the peptide does not affect the complex-forming abilities, or degree of incorporation, of this labeled peptide **9**. In contrast, when we repeated the FCS experiments with peptide **7**, in which the fluorophore is attached at the N terminus, it proved to be impossible to form complexes with high proportions of label included, as at even 5% label, the labeled peptide was preferentially displaced from the complex and increasing amounts were detected in solution (data not shown).

Fluorescence Quenching. Having established that LID complexes incorporating fluorophore-labeled lipid and peptide components could be formed without significant perturbation of the structure, we then carried out a series of fluorescence quenching experiments on such complexes bearing the same, or similar, fluorophores. These experiments were performed to determine which components, and indeed which parts of the individual components, were accessible at the surface of the complex or, conversely, shielded within the complex. Control experiments were carried out using acrylamide to quench peptide **8** (Mca-labeled), the Trp residue of unlabeled peptide **3**, Cy5-labeled plasmid, and BODIPY-labeled lipid **5** (where the labeled lipids make up 10% of the total lipid content). We then formulated a series of complexes with either the Cy5-labeled plasmid (LID*) or the Mca-labeled peptide **8** (LI*D) or the BODIPY-labeled lipid **5** [L*ID (DOPE)]. As the CRRETAWAC targeting domain of peptide **3** has an intrinsic fluorescence due to the presence of the Trp residue, we also investigated the quenching of the Trp fluorescence in LID complexes. In each case, the results gave standard linear Stern−Volmer plots

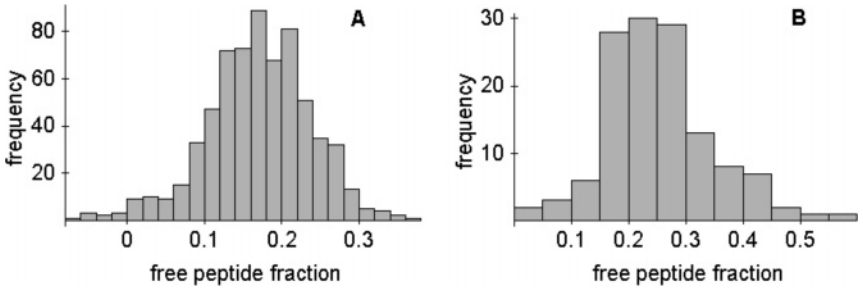

FIGURE 3: Histograms showing fraction of free peptide for complexes formulated in various percentages of labeled peptide **9** at (a) a 4:1 peptide/DNA charge ratio and (b) a 3:1 peptide:DNA charge ratio.

Table 4: Diffusion Times and Percentage of Species for Free Peptide **9** and Labeled LI*D Complex, Formulated at a 3:1 Charge Ratio

	component I (peptide **9**)		component II			
% labeled peptide **9**	diff time 0.22 ms I (%)	SE	diff time II (ms)	SE	II (%)	no. of measurements
0.1	17.7	1.7	3.98	0.22	82.3	18
0.5	15.8	0.5	2.97	0.07	84.2	120
1.0	17.5	0.6	3.21	0.06	82.5	120
5.0	20.5	0.6	2.34	0.05	79.5	134
10.0	12.2	0.8	2.21	0.05	87.8	77
20.0	16.9	0.5	2.41	0.04	83.1	189

with various gradients, indicating the degree of accessibility to the acrylamide quencher. The Cy5 label on the plasmid DNA was clearly much less accessible to acrylamide when complexed in the LID system (Figure 4a). A similar trend was observed for the Mca-labeled peptide **8** (Figure 4b); however, the decrease in the Stern−Volmer plot of the LI*D complex containing **8**, compared with the Stern−Volmer plot for **8** alone, was much less pronounced in this instance. The quenching results for the Trp residue on unlabeled peptide **3**, however, gave a steeper gradient on the Stern−Volmer plot for the formulated LID complex compared to the control experiment (Figure 4c), whereas the BODIPY-DOPE **5** produced a virtually identical set of results (Figure 4d). All Stern−Volmer plots gave trendlines with high R^2 regression values (0.9630−0.9989) with unforced *y*-intercepts.

Size of LID Complexes: FCS, PCS, and Freeze−Fracture EM. From the values of τ obtained from measurements of the lipid-labeled LID complexes (4.32−6.53 ms for the DOTMA-labeled complex and 3.79−5.12 ms for the DOPE-labeled complex) and of the peptide-labeled LID complexes (3.48−3.56 ms for the 4:1 complex and 2.21−3.98 ms for the 1.5:1 complex) we can derive the radii of the LID complexes, using eqs 5−7. This gives radii in the range of 30−45 nm. As a first step toward determining the macromolecular arrangement of the lipid, peptide, and DNA components within the vector, we studied the size of Lipofectin alone and also of DNA/peptide complexes with no added lipid. The Lipofectin (L) particles were also formulated by incorporating 5% of labeled DOTMA **6**. FCS measurements were carried out as before, the data were processed using a single-component model, and the resulting value of τ [0.375 (0.023), five measurements] was used to derive the particle diameter (Table 5). We also carried out a series of particle size determinations of various complexes using DLS. DLS has previously been used to determine the sizes of LID complexes (*58*, *59*) and of LD complexes (0.75:1 L/D weight ratio) with no peptide present (*57*). We have used the technique to determine the size of Lipofectin alone (L) and ID complexes. We have also tabulated the relative sizes of the various particles previously obtained by AFM (*11*) and by freeze−fracture EM measurements (Table 5).

The overall trends in size between the various complexes are consistent between the various techniques; however, the absolute values differ depending on the technique used. This arises because of the heterogenicity of the LID formulation, which, although mainly consisting of small, discrete particles, also includes large aggregates. These aggregates are recorded by DLS, thus making the average particle size observed larger; the very large aggregates are not detected by FCS (or discarded during data analysis), thus reducing the average particle size; and in AFM and freeze−fracture EM the aggregates can be discounted by simple inspection.

Morphology and Size of Complexes by Freeze−Fracture EM. Freeze−fracture electron micrographs were taken from several freeze−fracture preparations of each sample, and the sizes of the spherical structures measured (Table 5). Freeze−fracture electron micrographs of Lipofectin in water alone (L) (Figure 6a) show relatively large spheres (average diameter around 250 nm), which clearly display convex and concave fracture faces (shadows behind and in front of the structures, respectively) in a manner typical for bilayer vesicles such as liposomes (*58*). Because of their positive charge, they are separated from each other and do not form aggregates.

Freeze−fracture electron micrographs of lipoplexes (LD, L/D 4:1 by weight) (Figure 6b) visualize high concentrations of spherical particles with average diameters of 50 nm. Because these spherical particles display their shadow behind the structures exclusively, they are different from bilayer structures such as liposomes (Figure 6a) and represent "hard-core" particles (inset in Figure 6b). These LD hard-core particles appear to be mostly monomeric or small-numbered aggregates.

$K_{16}D$ polyplexes [truncated peptide/DNA complexex (K_{16}/D 1.7:1 by charge)] in freeze−fracture electron micrographs (Figure 6c) also show hard-core particles (average diameter around 50 nm) including presumably totally condensed DNA and additionally some evidence of partially condensed DNA (inset in Figure 6c). These $K_{16}D$ particles appear to be monomeric or small-numbered aggregates.

Freeze−fracture electron micrographs of lipopolyplexes of two types such as LID (I/D ratio 1.7:1 by charge) in Figure 7a and $LK_{16}D$ (truncated lipopolyplexes, in Figure 7b,c again show high concentrations of spherical hard-core particles

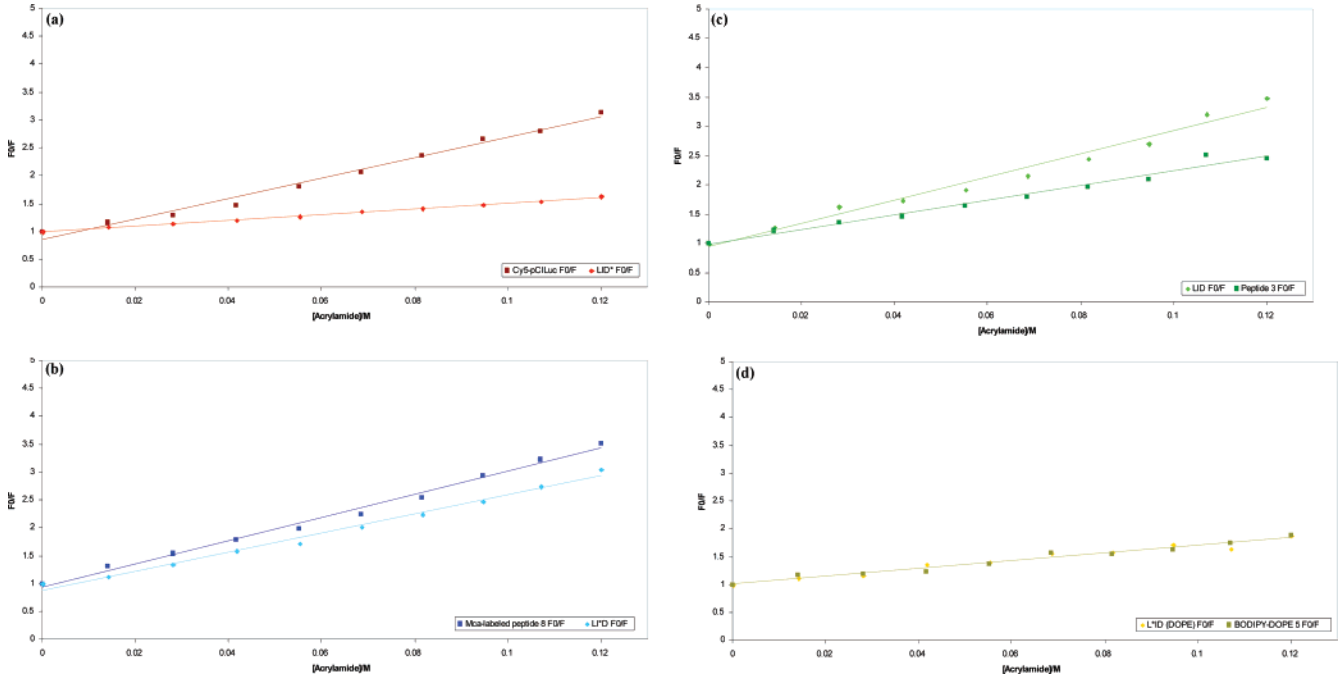

FIGURE 4: Stern−Volmer plots for (a) quenching of Cy5-pCILuc and LID* complex, (b) quenching of Mca-labeled peptide **8** and LI*D complex, (c) quenching of peptide **3** and LID complex, and (d) quenching of BODIPY-DOPE **5** and L*ID (DOPE) complex with 2 M acrylamide.

Table 5: Comparison of Sizes of LID Complexes, and Various Combinations of the Components, from DLS, FCS, AFM (*11*), and Freeze−Fracture EM Measurements[a]

	particle diameter (nm)			
	by DLS	by FCS	by AFM	by EM[b]
LID	150	60−90	44	30 (15−80)
L	358	80	nd	250 (50−600)
LD	209	nd	fibrous networks	50 (30−150)
ID	189	nd	44	30 (20− 0)
$LK_{16}D$	nd	nd	nd	30 (15−80)

[a] nd, not determined. [b] Size range of nonaggregated particles is given in parentheses.

displayed as monomers and smaller aggregates. The average diameters of both lipopolyplex types are smaller (30 nm) than the diameter of the lipoplexes (LD 50 nm) (Table 5). Additionally, in Figure 7a quite a number of residual liposomes (some of them marked by L) are visible. Superficially, the hard-core particles observed in the lipoplex samples and created by lipid-condensed DNA (Figure 6b) seem to be similar to those detectable in Figure 7a−c for the LID and $LK_{16}D$ complexes (i.e., peptide/lipid-condensed DNA), but they are not. Especially the $LK_{16}D$ lipopolyplexes show frequently "fuzzy" (inset in Figure 7b) and/or dotted boundaries (inset in Figure 7c), leading to an outer shell/inner core appearance marked by ↔ and ↓, respectively.

DISCUSSION

In the original study of the LID system (*11*), it was established that the complex undergoes receptor-mediated endocytosis, indicating a spatial arrangement with the integrin-recognition portion (CRRETAWAC) of peptide **3** able to interact with cell surface receptors. The polylysine part of the peptide clearly also serves to condense the plasmid DNA, resulting in discrete particles, which were visualized by AFM. In contrast, complexes formed from Lipofectin and DNA alone (LD) were shown by AFM to form fibrous networks, and these complexes exhibited much lower transfection efficiencies. However, Lipofectin also plays an important role, as complexes formed from peptide and DNA (ID) alone also had much lower transfection efficiencies. Lipofectin may play a role both in mediating endosomal escape of the internalized LID complex and in reducing the degradation of the plasmid DNA. The latter observation points to a shielding of the LID complex by the lipid components.

The initial aim of this research was to establish, using FCS, the exact composition of the LID complexes and their sizes. It is clear from the results presented that both lipids, DOTMA and DOPE, are incorporated into the LID complex in a 1:1 ratio, at close to the stoichiometry of mixing. If we assume, on the basis of the size distribution of the complexes, that each LID particle contains only a single plasmid DNA molecule, this implies that each complex includes around 3000 lipid molecules. However, at a peptide/DNA charge ratio of 4:1, a significant proportion of the peptide is not incorporated into the complex. Although the 4:1 charge ratio gave optimum transfection efficiencies in a range of cell lines, both *in vitro* and *in vivo* (*11*), zeta potential measurements and PicoGreen fluorescence assays have recently indicated that stable, transfection active LID complexes are actually formed at a 1.5:1 peptide/DNA charge ratio (*57*), and no change in the zeta potential or particle stabilities occurs beyond this charge ratio. Indeed, when we repeated the FCS experiments at a 1.5:1 peptide/DNA charge ratio, about 85% of the peptide was incorporated into the complex. This in turn indicates that the LID complex itself includes around 750 peptide molecules.

The observation that not all of peptide **9** is incorporated at a 4:1 charge ratio does not appear to be a perturbation introduced by the presence of the fluorophore, as the level of peptide incorporation is independent of the percentage of

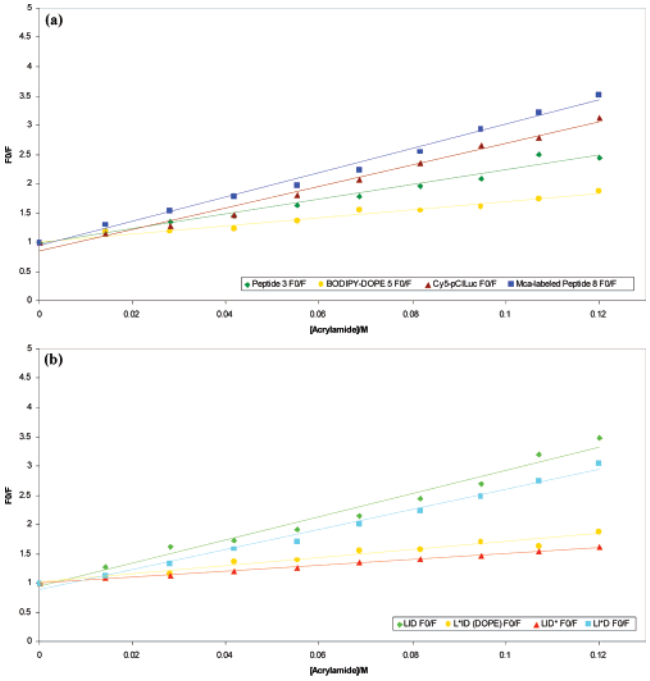

FIGURE 5: Stern−Volmer plots for (a) quenching of various fluorophores in control experiments and (b) quenching of various fluorophores in LID systems with 2 M acrylamide.

labeled peptide present. Furthermore, the nature and position of the fluorophores attached to the lipid components appears to be of minor importance, as the incorporation of the lipid components is almost complete at this formulation. This contrasts with previous work (*25*) in which the size of fluorophore-labeled micelles was measured by FCS and that of unlabeled micelles by DLS. In these experiments it was found that the fluorophore was of comparable magnitude to the micelle and made a significant difference in the measured size of the micelle. As the LID particles are larger and more complex than micelles, attachment of fluorescent labels represents less of a perturbation to the size of the complex as a whole. However, the position and nature of the attached fluorophore is crucially important in some instances for the correct formation of the LID complex. With peptide **7**, in which the fluorophore was attached at the N terminus, it proved to be impossible to form complexes with high proportions of label included: clearly the Texas Red label is too large to be accommodated within the condensed plasmid DNA/peptide part of the complex.

With the stoichiometry of the LID complex established, the fluorescence quenching studies enabled us to shed some light on the possible spatial arrangement of the individual components within the complex. The difference between the quenching results for the Cy5-pCILuc control and LID* experiments, for which the Stern−Volmer plot gave a much shallower gradient on the latter (Figure 4a), clearly showed that the DNA component is internal to the complex. This is entirely consistent with the observation (*11*) that the LID formulation shields the plasmid DNA from enzymatic degradation *in vivo* and *in vitro*.

We then examined the quenching of fluorophores on the integrin-binding portion of the peptide. When peptide **8** was used, in which the Mca label is attached to the C terminus, there was a slight decrease in fluorophore accessibility when the peptide was formulated in the complex (Figure 4b). This might imply a situation whereby the peptide C terminus was partially coated with, and hence only slightly shielded by, the lipid components of the formulation. In contrast, when the quenching of the (intrinsic fluorophore) Trp residue was investigated (Figure 4c), the LID system was more easily quenched compared to peptide **3** alone in solution. This implies that the cyclic portion of peptide **3** adopts a more exposed (and therefore potentially more ordered) spatial arrangement within the LID complex compared to its inherent folding in solution. The observation made for peptides **3** and **8** strongly suggests that the integrin-binding domain, which plays a crucial role in the transfection process, is accessible at the surface of the particle. When peptide **3** was replaced by a truncated K_{16} peptide to give a $LK_{16}D$ formulation, the transfection efficiency was reduced 6-fold (*11*), implying that the majority of the internalization takes place via an endocytotic mechanism dependent on the interaction between the CRRETAWAC domain and $\alpha_5\beta_1$ integrins on the cell surface. If both the DNA and the peptide were completely enveloped by the lipid, a two-stage mechanism would have to be postulated, whereby (nonspecific) fusion between the cell membrane and the lipid component on the LID complex would subsequently reveal the CRRETAWAC domain, allowing a receptor-specific interaction to take place. There is some precedent for this: for example, it has been reported that cypovirus particles can be completely coated with Lipofectin (as shown by cryoelectron microscopy) with the infectivity of these particles being significantly enhanced thereby (*60*). However, such a model is not consistent with the results from the quenching of the Trp residue (Figure 4c), which show this residue, at least, to be accessible to quenchers.

The quenching of fluorophores positioned on the lipid components afforded further insights into the arrangement of the complex and the effects of site-specific labeling. In an ordered bilayer structure it would be expected that lipids labeled in the lipophilic portion, as in BODIPY-labeled DOPE **5**, would have the fluorophore buried within the bilayer and therefore not accessible to quenchers. The virtually identical results for the control and L*ID (DOPE) experiments suggested that in each case the fluorophore was buried within a (bi)layer structure and is therefore much less accessible to the acrylamide quencher (Figure 4d). The fact that it was not completely shielded from the quencher (which would yield nearly horizontal Stern−Volmer plots) would suggest an irregular lipid layer. In contrast, fluorescence quenching experiments on lipid **6** (DOTMA with the fluorophore label attached to the headgroup) showed poor quenching properties (data not shown). This probably reflects the tendency of the charged fluorophore to fold back on itself within the liposome, and no further experiments were therefore carried out on this lipid.

Overall, the fluorescence quenching results are summarized by Figure 5. In the LID system, the accessibility of the fluorophores to collisional quenchers could be arranged in the following order: Trp on peptide **3** > Mca on peptide **8** > BODIPY on lipid **5** > Cy5 on pCILuc (Figure 5b).

Turning next to the freeze−fracture EM studies, the Lipofectin (L) morphology displayed in Figure 6a corresponds with bilayer vesicles such as liposomes (*59*). However, when LD complexes are formed (Figure 6b) hard-core particles are observed. The majority of lipoplex structures

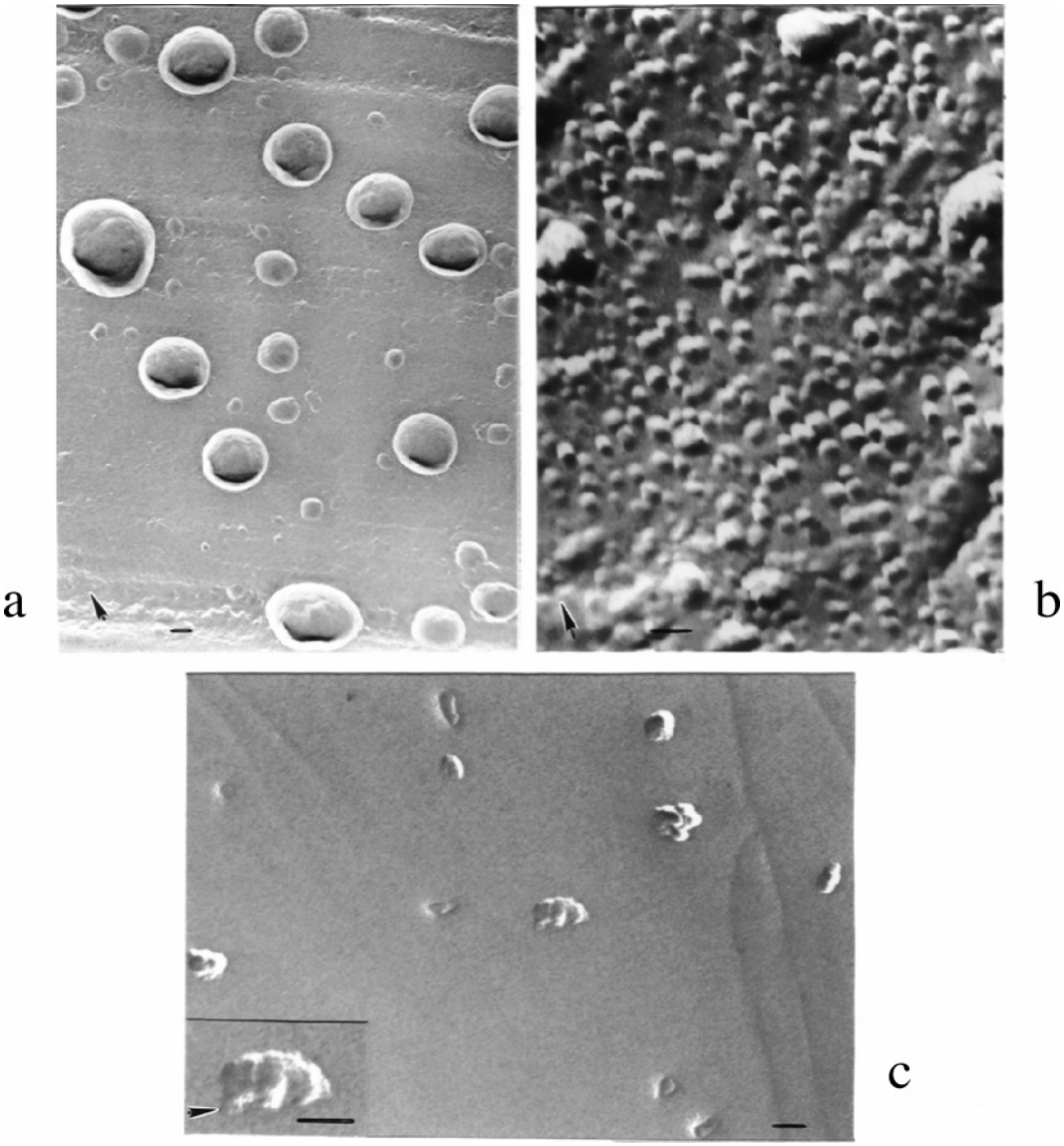

FIGURE 6: Freeze−fracture electron micrographs of (a) Lipofectin (L) alone in water, (b) lipoplex (LD) complex, and (c) polyplex ($K_{16}D$) complex. The bar on all electron micrographs represents 100 nm, and the shadow direction is marked by an arrow (↑).

previously studied by freeze−fracture EM and/or cryoelectron microscopy techniques have been shown to adopt a wide variety of bilayer-containing superstructure morphologies. Bilayer structures such as liposome-beads on DNA strings (*37*), supercoiled plasmid DNA coated by a bilayer tubule (spaghetti) in coexistence with bilayer-containing meatball complexes (*15*, *30*, *32*), bilayer-containing particles (*38*), multilamellar arrangements with the DNA sandwiched between lipid (*16*, *18*, *19*, *20*, *39*), and invaginated liposomes (*32*, *40*) have been observed. Furthermore, lipid-containing structures not arranged in a bilayer version have been detected, including condensed liposome/DNA complexes with additional spikes (*17*) or map-pin structures (*34*). Additionally, non-bilayer LD arrangements have also been observed including hexagonal (H_{II} or honeycomb-type) structure (*30*−*32*, *34*, *41*) or cubic lipid phases (*42*). As previously shown, the formation of LD superstructures is strongly dependent upon the lipid valence, the proportion and type of helper lipids, the charge ratio of lipid to DNA, the ionic strength of the medium, and the type of the oligonucleotide/DNA component (*30*, *32*, *43*). Under the conditions investigated here (1.2 μg/680 nmol of DNA/Lipofectin ratio in water) the lipoplex displays hard-core particles instead of spaghetti/meatball complexes as previously described for Lipofectin, complexed with supercoiled plasmid DNA at a 1.2 μg/20 nmol DNA/Lipofectin ratio (*30*, *32*). In Figure 6b no bilayer structures are detectable, but hard-core particles that are significantly smaller in size than the liposomes (Figure 6a) are, indicating a high degree of lipid-mediated condensation of the DNA.

$K_{16}D$ polyplexes in freeze−fracture electron micrographs (Figure 6c) also show hard-core particles (average diameter around 50 nm) including presumably totally condensed DNA similar to previously described peptide-condensed DNA particles (*61*). Additionally, structures are detected giving evidence of partially condensed DNA (inset in Figure 6c).

Freeze−fracture electron micrographs of the LID and $LK_{16}D$ lipopolyplex particles (Figure 7a−c) show an even greater extent of condensation of the DNA by combining the compacting "power" of the cationic lipid *and* the cationic peptide. Similar to previous spermidine/cationic lipid condensation attempts (*34*), highly condensed and even smaller

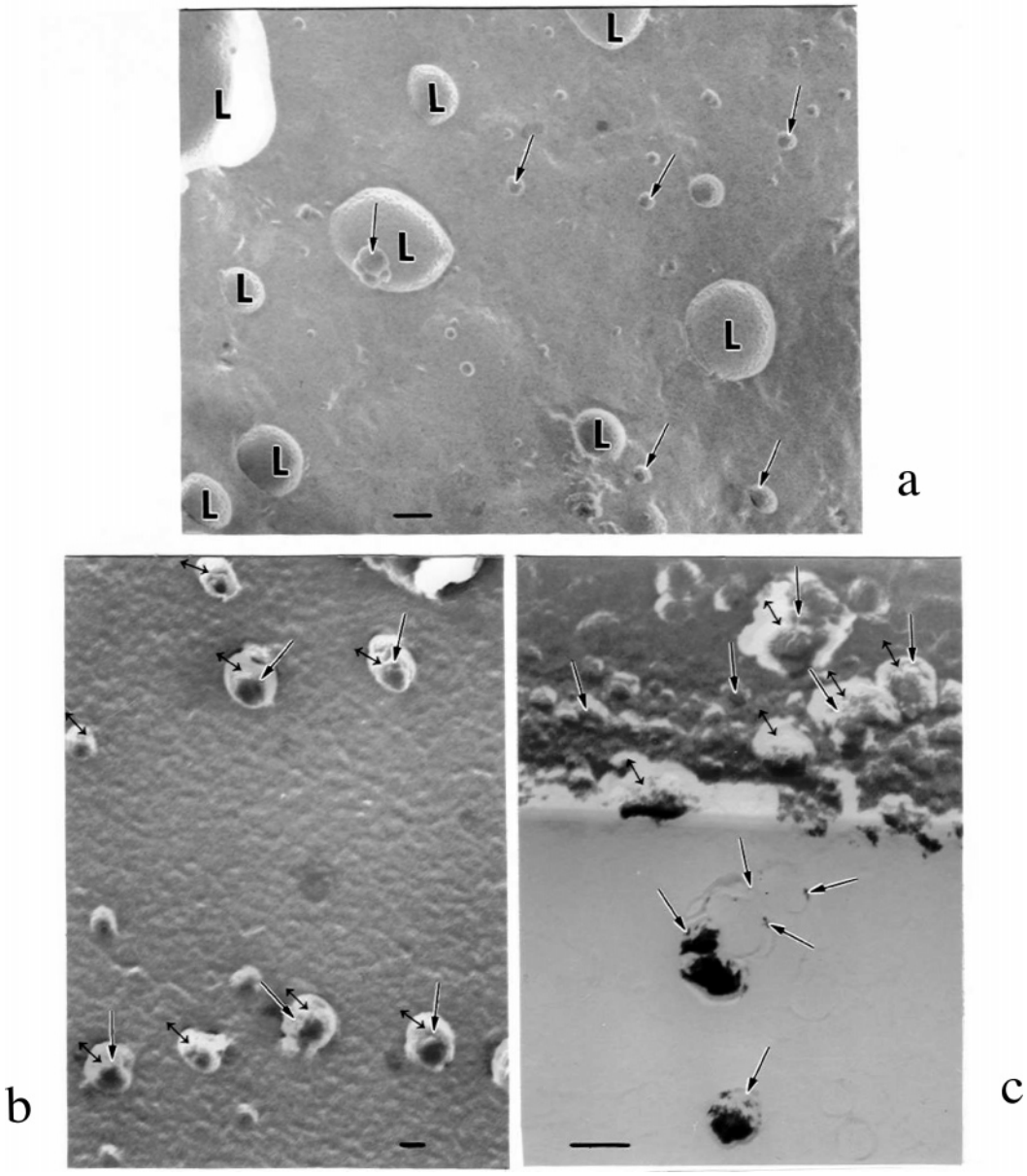

FIGURE 7: Freeze−fracture electron micrographs of (a) lipopolyplex (LID) complex and (b, c) of lipopolyplex ($LK_{16}D$) complex. The bar on all electron micrographs represents 100 nm, and the shadow direction is running from bottom to top. In (a) L marks some of the residual liposomes. Some of the "fuzzy" and/or dotted boundaries are marked by ↔ and ↓, respectively.

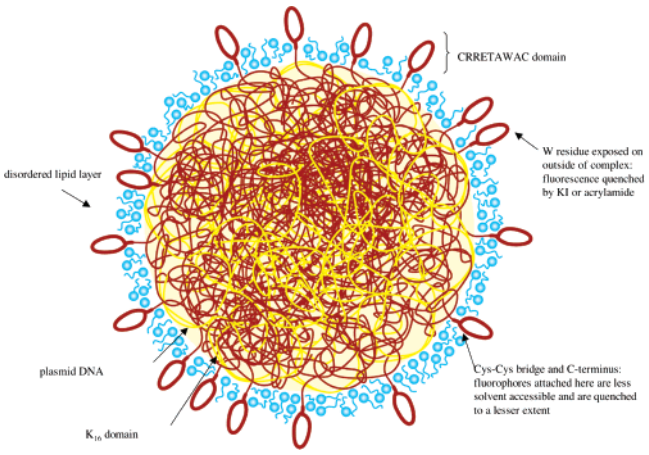

FIGURE 8: Model for the macromolecular organization of the LID vector.

particles than the LD complexes are obtained. Furthermore, in contrast to the LD complexes, freeze−fracture electron micrographs taken from LID (Figure 7a) but especially from $LK_{16}D$ preparations (Figure 7b,c) suggest evidence for a particle structure displaying a "hard" inner core, surrounded by an irregular, "fuzzy" outer shell. Such inner "hard" core/outer soft-shell particles have been observed previously (*21*) in preparations made of adenovirus core peptide (μ) and plasmid DNA added to cationic liposomes formed from DC-Chol/DOPE. These were studied by cryo-EM. These μ/DNA polyplex complexes formed hard-core particles; however, on addition of the DC-Chol/DOPE liposomes these hard-core particles were seen to be encapsulated within a cationic bilayer structure. In contrast, the Lipofectin used in our work appears to form an irregular layer at the periphery of the hard core. The greater steric bulk of the DC-Chol and the different sequence of the μ peptide (which lacks a receptor-binding moiety) may account for this difference in morphology. The irregular, "soft" outer shell observed for LID and $LK_{16}D$ (Figure 7a−c) is also consistent with the quenching

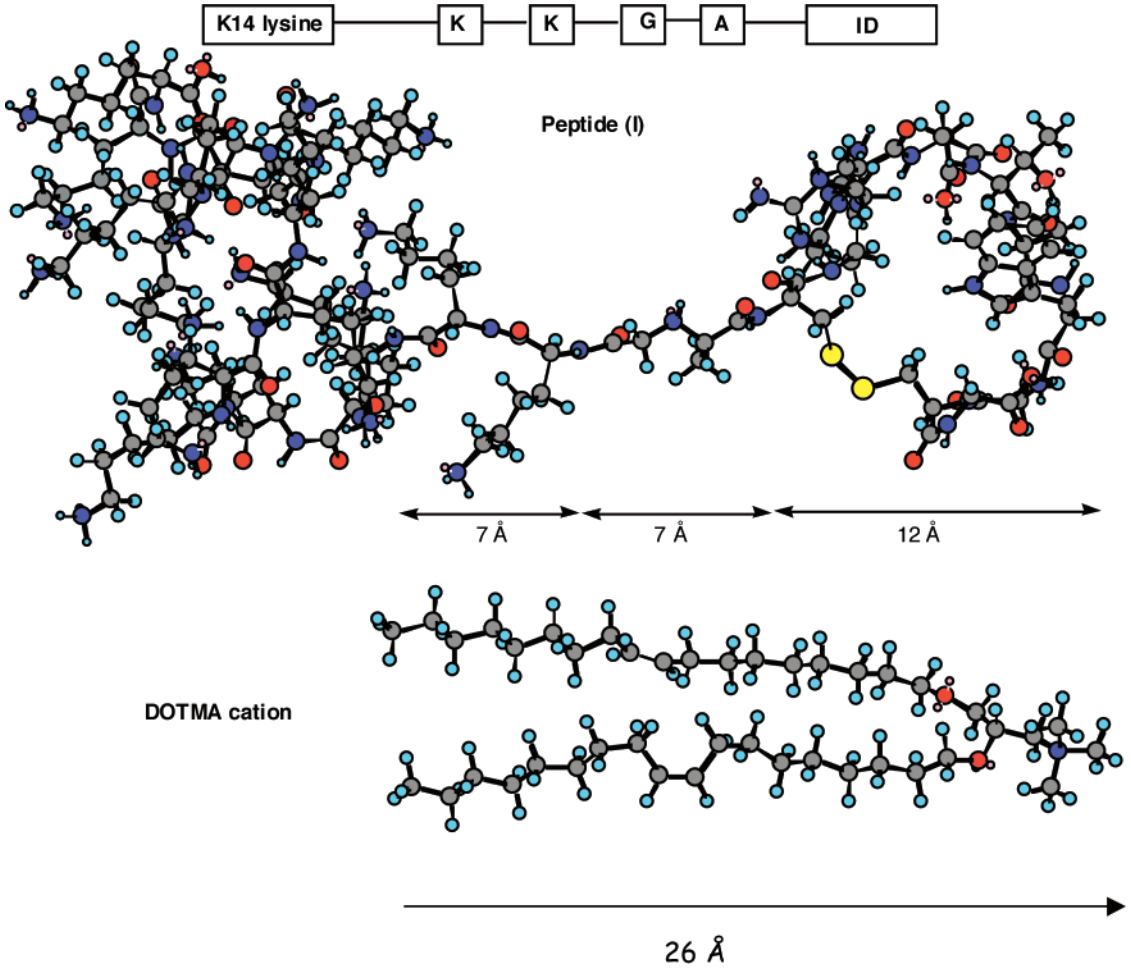

FIGURE 9: Relative dimensions of the CRRETAWAC domain, the linker, and DOTMA.

experiments with fluorophore labeled lipid **5** described earlier, which again points to an irregular lipid layer coating an inner hard-core structure.

The relative particle sizes of L, LD, ID, and LID complexes observed by freeze−fracture EM are consistent with those observed by DLS (Table 5). The Lipofectin particles (L) are significantly larger than the complexes. Complexation of Lipofectin with DNA gives LD particles in which the DNA has been partially condensed by the lipid; however, a much greater degree of condensation is seen when the DNA is condensed by the peptide (ID). Again, when both the cationic lipid and the peptide are combined (LID), the smallest and most compact structures are seen.

On the basis of these studies, we can therefore postulate a model for the LID complex. The cationic (K_{16}) portion of the peptide, I, as expected interacts with the plasmid DNA, resulting in a tightly condensed DNA/peptide inner core. The quenching experiments indicate that the DNA is mostly shielded from the solvent, probably by both the peptide and electrostatic interactions with the lipid, and both the freeze−fracture EM studies and quenching studies with fluorophore-labeled lipids indicate that the lipids are likely to be present as a disordered coating of the particle, further condensing the structure but not forming ordered monolayer, bilayer, or multilamellar structures. The resolution of freeze−fracture EM is determined by the size of the evaporated Pt/C particles forming the replica and is, in our hands, limited to 2 nm for periodical structures (*59*). Therefore, higher resolution techniques such as negative staining and/or cryoelectron microscopy would have to be employed to elucidate the fine structure of the lipid coat.

Finally, the different quenching results obtained when a fluorophore is attached to the C terminus of the peptide (peptide **8**) versus those obtained using the intrinsic fluorescence of the Trp residue of peptide **3** (Figure 5b) suggest a structure in which the CRRETAWAC domain is predominantly exposed at the lipid surface (Figure 8). The cyclic structure of this cystine-bridged domain imparts a turn (*62*), which will have the effect of directing the C terminus back toward the DNA-condensing domain. A fluorophore attached to the C terminus will therefore be slightly buried within the lipid layer and hence less accessible to quenchers. The inaccessibility to quenching species (such as acrylamide) of peptides bearing fluorophores buried within a lipid membrane has been previously noted in studies of the orientation of the peptide antibiotic, nisin, within artificial membranes (*63*). Conversely, the portion of the CRRETAWAC domain that actually binds to the integrin—including the Trp residue itself—will protrude from the disordered lipid coating and will therefore be fully accessible to the quencher, as well as to the cell surface receptors. We have carried out preliminary modeling studies (Figure 9), and it should be noted that the very small number of amino acids between the Lys_{16} and CRRETAWAC domains of peptide **3** (i.e., Gly and Ala) may

not form a linker of sufficient length to allow the CRRETAWAC domain to protrude fully from even the disordered lipid layer postulated here, let alone through an ordered lipid bilayer.

In summary, the biophysical experiments described here have enabled us to formulate a detailed model for the stoichiometry and macromolecular organization of this integrin-targeted, ternary lipopolyplex gene delivery vector. The study has shown the usefulness of the different techniques and also their complementarity to present a more complete picture of the macromolecular organization than could have been gained from the use of one approach alone. It also underscores the value of specific, regioselective fluorophore labeling of peptides and lipids in carrying out FCS and fluorescence quenching experiments. Finally, on the basis of the postulated model for the LID complex, it will be possible to design more efficient targeted transfection complexes with greater *in vivo* stability, and we have already started to modify and enhance the lipid and peptide components to address these issues (*64*−*66*).

ACKNOWLEDGMENT

We thank Dr. Piers Gaffney (Imperial College London) for a generous gift of Cy3 iodoacetamide and for the procedure for the synthesis of Cy3 iodoacetamide prior to publication. We also thank Dr. Philippe Bastiaens (EMBL, Heidelberg) and Dr. Jagdish Rao (Cancer Research U.K.) for many helpful and insightful discussions. We are grateful to Dr. Paul Rothwell, Dr. Tina Daviter, and the ISMB Biophysics Centre for access to the FluoroMax and countless discussions on fluorescence quenching, as well as to David Smithson (ICH) for Figure 8.

SUPPORTING INFORMATION AVAILABLE

Representative Mathematica output file for the analysis of the FCS data from the LID complex, formulated at a 1.5:1 peptide/DNA charge ratio, containing different percentages of Cy3 labeled peptide **9**. This material is available free of charge via the Internet at http://pubs.acs.org.

REFERENCES

1. Somia, N., and Verma, I. M. (2000) Gene therapy: trials and tribulations, *Nat. Rev. Genet. 1*, 91−99.
2. Marshall, E. (1999) Clinical trials−gene therapy death prompts review of adenovirus vector, *Science 286*, 2244−2245.
3. Kang, E. M., and Tisdale, J. F. (2004) The leukaemogenic risk of integrating retroviral vectors in hematopoietic stem cell gene therapy applications, *Curr. Hematol. Rep. 3*, 274−281.
4. Tranchant, I., Thompson, B., Nicolazzi, C., Mignet, N., and Scherman, D. (2004) Physicochemical optimization of plasmid delivery by cationic lipids, *J. Gene Med. 6*, S24−S35.
5. Bloque, C., Fabre, E., Bureau, M. F., and Scherman, D. (2004) Plasmid DNA electrotransfer for intracellular and secreted proteins expression: new methodological developments and applications, *J. Gene Med. 6*, S11−S23.
6. Mumper, R. J., and Cui, Z. (2003) Genetic immunization by jet injection of targeted pDNA-coated nanoparticles, *Methods 31*, 255−262.
7. Davis, M. E. (2002) Non-viral gene delivery systems, *Curr. Opin. Biotechnol. 13*, 128−131.
8. Miller, A. D. (1998) Cationic liposomes for gene therapy, *Angew. Chem., Int. Ed. Engl. 37*, 1769−1785.
9. Wolff, J. A. (2002) The "grand" problem of synthetic delivery, *Nat. Biotechnol. 20*, 768−769.
10. Varga, C. M., Wickham, T. J., and Lauffenburger, D. A. (2000) Receptor-mediated targeting of gene delivery vectors: insights from molecular mechanisms for improved vehicle design, *Biotechnol. Bioeng. 70*, 593−605.
11. Hart, S. L., Arancibia-Cárcamo, C. V., Wolfert, M. A., Mailhos, C., O'Reilly, N. J., Ali, R. R., Coutelle, C., George, A. J. T., Harbottle, R. P., Knight, A. M., Larkin, D. F. P., Levinsky, R. J., Seymour, L. W., Thrasher, A. J., and Kinnon, C. (1998) Lipid-mediated enhancement of transfection by a nonviral integrin-targeting vector, *Hum. Gene Ther. 9*, 575−585.
12. Hart, S. L., Collins, L., Gustafsson, K., and Fabre, J. W. (1997) Integrin-mediated transfection with peptides containing arginine-glycine-aspartic acid domains, *Gene Ther. 4*, 1225−1230.
13. Jenkins, R. G., Herrick, S. E., Meng, Q.-H., Kinnon, C., Laurent, G. J., McAnulty, R. J., and Hart, S. L. (2000) An integrin-targeted non-viral vector for pulmonary gene therapy, *Gene Ther. 7*, 393−400.
14. Parkes, R., Meng, Q. H., Siapati, K. E., McEwan, J. R., and Hart, S. L. (2002) High efficiency transfection of porcine vascular cells in vitro with a synthetic vector system, *J. Gene Med. 4*, 292−299.
15. Sternberg, B., Sorgi, F. L., and Huang, L. (1994) New structures in complex formation between DNA and cationic liposomes visualized by freeze−fracture electron microscopy, *FEBS Lett. 356*, 361−366.
16. Rädler, J. O., Kotover, I., Salditt, T., and Safinya, C. R. (1997) Structure of DNA−cationic liposome complexes: DNA intercalation in multilamellar membranes in distinct interhelical packing regimes, *Science 275*, 810−814.
17. Xu, Y., Hui, S.-W., Frederik, P., and Szoka, F. C. (1999) Physicochemical characterization and purification of cationic liposomes, *Biophys. J. 77*, 341−353.
18. Pitard, B., Oudrhiri, N., Vigneron, J.-P., Hauchecorne, M., Aguerre, O., Toury, R., Airiau, M., Ramasawmy, R., Scherman, D., Crouzet, J., Lehn, J.-M., and Lehn, P. (1999) Structural characteristics of supramolecular assemblies formed by guanidinium-cholesterol reagents for gene transcription, *Proc. Natl. Acad. Sci. U.S.A. 96*, 2621−2626.
19. Schmutz, M., Durand, D., Debin, A., Palvadeau, Y., Etienne, A., and Thierry, A. R. (1999) DNA packing in stable lipid complexes designed for gene transfer imitates DNA compaction in bacteriophage, *Proc. Natl. Acad. Sci. U.S.A. 96*, 12293−12298.
20. Bell, P. C., Bergsma, M., Dolbnya, I. P., Bras, W., Stuart, M. C. A., Rowan, A. E., Feiters, M. C., and Engerts, J. B. F. N. (2003) Transfection mediated by gemini surfactants: engineered escape from the endosomal compartment, *J. Am. Chem. Soc. 125*, 1551−1558.
21. Tagawa, T., Manvell, M., Brown, N., Keller, M., Perouzel, E., Murray, K. D., Harbottle, R. P., Tecle, M., Booy, F., Brahimi-Horn, M. C., Coutelle, C., Lemoine, N. R., Alton, E. W. F. W., and Miller, A. D. (2002) Characterization of LMD virus-like nanoparticles self-assembled from cationic liposomes, adenovirus core peptide μ (mu) and plasmid DNA, *Gene Ther. 9*, 564−576.
22. Thompson, N. L., Lieto, A. M., and Allen, N. W. (2002) Recent advances in fluorescence correlation spectroscopy, *Curr. Opin. Struct. Biol. 12*, 634−641.
23. Hess, S. T., Huang, S., Heikal, A. A., and Webb, W. W. (2002) Biological and chemical applications of fluorescence correlation spectroscopy: a review, *Biochemistry 41*, 697−705.
24. Haustein, E., and Schwille, P. (2003) Ultrasensitive investigations of biological systems by fluorescence correlation spectroscopy, *Methods 29*, 153−166.
25. Bastiaens, P. I. H., Pap, E. H. W., Borst, J.-W., van Hoek, A., Kulinski, T., Rigler, R., and Visser, A. J. W. G. (1993) The interaction of pyrene-labeled diacylglycerol with protein-kinase C in mixed micelles, *Biophys. Chem. 48*, 183−191.
26. Hink, M. A., van Hoek, A., and Visser, A. J. W. G. (1999) Dynamics of phospholipid molecules in micelles: characterization with fluorescence correlation spectroscopy and time-resolved fluorescence anisotropy, *Langmuir 15*, 992−997.
27. Nörenberg, R., Klingler, J., and Horn, D. (1999) Study of the interactions between poly(vinyl pyrrolidone) and sodium dodecyl sulfate by fluorescence correlation spectroscopy, *Angew. Chem., Int. Ed. Engl. 38*, 1626−1629.
28. Van Rompaey, E., Engelborghs, Y., Sanders, N., De, Smedt, S. C., and Demeester, J. (2001) Interactions between oligonucleotides and cationic polymers investigated by fluorescence correlation spectroscopy, *Pharm. Res. 18*, 928−936.
29. Delie, F., Gurny, R., and Zimmer, A. (2001) Fluorescence correlation spectroscopy for the characterization of drug delivery systems, *Biol. Chem. 382*, 487−490.

30. Sternberg, B. (1996) Morphology of cationic liposome/DNA complexes in relation to their chemical composition, *J. Liposome Res. 6*, 515−533.
31. Sternberg, B. (1996) Liposomes as a model for membrane structures and structural transformations: a liposome album, in *Handbook of Nonmedical Applications of Liposomes, Vol. IV: From Gene Delivery and Diagnostics to Ecology* (Larsic, D., and Barenholz, Y., Eds.) pp 271−297, CRC Press, Boca Raton, FL.
32. Sternberg, B. (1998) Ultrastructural morphology of cationic liposome−DNA complexes for gene therapy, in *Medical Applications of Liposomes* (Lasic, D. D., and Papahadjopoulos, D., Eds.) pp 395−427, Elsevier, Amsterdam, The Netherlands.
33. Meyer, O., Kirpotin, D., Hong, K., Sternberg, B., Park, J. W., Woodle, M. C., and Papahadjopoulos, D. (1998) Cationic liposome coated with poly (ethylene glycol) as carriers for oligonucleotides, *J. Biol. Chem. 273*, 15621−15627.
34. Sternberg, B., Hong, K., Zheng, W., and Paphadjopoulos, D. (1998) Ultrastructural characterization of cationic liposome−DNA complexes showing enhanced stability in serum and high transfection activity *in vivo*, *Biochim. Biophys. Acta 1375*, 23−35.
35. Torchilin, V. P., Lukyanov, A. N., Gao, Z., and Papahadjopoulos-Sternberg, B. (2003) Immunomicelles: targeted pharmaceutical carriers for poorly soluble drugs, *Proc. Natl. Acad. Sci. U.S.A. 100*, 6039−6044.
36. Torchilin, V. P., Levchenko, T. S., Rammohan, R., Volodina, N., Papahadjopoulos-Sternberg, B., and D'Souza, G. G. (2003) Cell transfection *in vitro* and *in vivo* with nontoxic TAT peptide−liposome−DNA complexes, *Proc. Natl. Acad. Sci. U.S.A. 100*, 1972−1977.
37. Gershon, H., Ghirlando, R., Guttman, S. B., and Minsky, A. (1993) Mode of formation and structural features of DNA cationic liposome complexes used for transfection, *Biochemistry 32*, 7143−7151.
38. Gustafsson, J., Arvidson, G., Karlsson, G., and Almgreen, M. (1995) Complexes between cationic liposomes and DNA visualized by Cryo-TEM, *Biochim. Biophys. Acta 1235*, 305−312.
39. Lasic, D. D., Strey, H., Stuart, M. C. A., Podgornik, R., and Frederik, P. M. (1997) The structure of DNA−liposome complexes, *J. Am. Chem. Soc. 119*, 832−833.
40. Templeton, N. S., Lasic, D. D., Frederik, P. M., Strey, H. H., Roberts, D. D., and Pavlakis, G. N. (1997) Improved DNA: liposome complexes for increased systemic delivery and gene expression, *Nat. Biotechnol. 15*, 647−652.
41. Koltover, I., Salditt, T., Radler, J. O., and Safinya, C. R. (1998) An inverted hexagonal phase of cationic liposome−DNA complexes related to DNA release and delivery, *Science 281*, 78−81.
42. Mok, K. W. C., and Cullis, P. R. (1997) Structural and fusiogenic properties of cationic liposomes in the presence of plasmid DNA, *Biophys. J. 73*, 2534−2545.
43. Hurley, C. A., Wong, J. B., Hailes, H. C., and Tabor, A. B. (2004) Asymmetric synthesis of dialkyloxy-3-alkylammonium cationic lipids, *J. Org. Chem., 69*, 980−984.
44. Veber, D. F., Varga, S. L., Hirschmann, R., Milkowski, J. D., and Denkewalter, R. G. (1972) Acetamidomethyl−novel thiol protecting group for cysteine, *J. Am. Chem. Soc. 94*, 5456−5461.
45. Chan, H.-L., Gharbi, S., Gaffney, P. R. J., Cramer, R., Waterfield, M. D., and Timms, J. (2005) Proteomic analysis of redox- and ErbB2-dependent changes in mammary luminal epithelial cells using cysteine- and lysine-labeling two-dimensional difference gel electrophoresis, *Proteomics 5*, 2908−2926.
46. Fischer, R., Mader, O., Jung, G., Brock, R. (2003) Extending the applicability of carboxyfluorescein in solid-phase synthesis, *Bioconjugate Chem. 14*, 653−660.
47. Madge, D. E., Elson, E. L., and Webb, W. W. (1972) Thermodynamics fluctuations in a reacting system: measurement by fluorescence correlation spectroscopy, *Phys. Rev. Lett. 29*, 705−708.
48. Madge, D. E., Elson, E. L., and Webb, W. W. (1974) Fluorescence correlation spectroscopy. II. An experimental realization, *Biopolymers 13*, 29−61.
49. Visser, A. J. W. G., and Hink, M. A. (1999) New perspectives of fluorescence correlation spectroscopy, *J. Fluorescence 9*, 81−87.
50. Wohland, T., Rigler, R., and Vogel, H. (2001) The standard deviation in fluorescence correlation spectroscopy, *Biophys. J. 80*, 2987−2999.
51. Van de Hulst, H. C. (1957) *Light Scattering by Small Particles*, Wiley, New York.
52. Kerker, M. (1969) *The Scattering of Light and Other Electromagnetic Radiation*, 1st ed., Academic Press, New York.
53. Provencher, S. W. (1979) Inverse problems in polymer characterisation−direct analysis of polydispersity with photon correlation spectroscopy, *Makromol. Chem. 180*, 201−242.
54. Provencher, S. W. (1982) CONTIN−a general-purpose constrained regularization program for inverting noisy linear algebraic and integral-equations, *Comp. Phys. Com. 27*, 229−242.
55. Lakowicz, J. R. (1999) *Principles of Fluorescence Spectroscopy*, 2nd ed., Kluwer Academic/Plenum, New York.
56. Sarkar, S., Lee, L. K., Hart, S. L., Hailes, H. C., Levy, S. M., Tabor, A. B., and Ayazi, Shamlou, P. (2005) Fractal structure of polycation−DNA complexes, *Biotechnol. Appl. Biochem. 41*, 127−136.
57. Lee, L. K., Siapati, E. K., Jenkins, R. G., McAnulty, R. J., Hart, S. L., and Ayazi Shamlou, P. (2003) Biophysical characterization of an integrin-targeted non-viral vector for pulmonary gene delivery, *Med. Sci. Monit. 9*, BR 54−61.
58. Sarkar, S., Zhang, H., Levy, S. M., Hart, S. L., Hailes, H. C., Tabor, A. B., and Ayazi Shamlou, P. (2003) Prediction of size distribution of lipid-peptide-DNA vector particles using Monte Carlo simulation techniques, *Biotechnol. Appl. Biochem. 38*, 95−102.
59. Sternberg, B. (1993) Freeze−fracture electron microscopy of liposomes, in *Liposome Technology, 2nd ed., Vol. I: Liposome Preparation and Related Techniques* (Gregoriadis, G., Ed.) pp 363−383, CRC Press, Boca Raton, FL.
60. Hill, C. L., Booth, T. F., Stuart, T. I, and Mertens, P. P. C. (1999) Lipofectin increases the specific activity of cypovirus particles for cultured insect cells, *J. Virol. Methods 78*, 177−189.
61. Lee, R. J., and Huang, L. (1996) Folate-targeted, anionic liposome-entrapped polylysine-condensed DNA for tumor cell-specific gene transfer, *J. Biol. Chem. 271*, 8481−8487.
62. Ruoslahti, E. (1996) RGD and other recognition sequences for integrins, *Annu. Rev. Cell. Dev. Biol. 12*, 697−715.
63. Breukink, E., van Kraaij, C., van Dalen, A., Demel, R. A., Siezen, R. J., de Kruijff, B., and Kuipers, O. P. (1998) The orientation of nisin in membranes, *Biochemistry 37*, 8153−8162.
64. Writer, M. J., Hurley, C. A., Sarkar, S., Wong, J. B., Irvine, S., Afzal, F., Ho, J., Odlyha, M., McEwan, J. R., Lawrence, M. J., Tabor, A. B., Ayazi Shamlou, P., Hailes, H. C., and Hart, S. L. (2006) Systematic analysis and optimisation of the cationic lipid component of lipoplex and lipopolyplex formulations for efficient gene transfer, *J. Liposome Res. 16*, 373−389.
65. Pilkington-Miksa, M. A., Writer, M. A., Sarkar, S., Meng, Q.-H., Barker, S. E., Ayazi Shamlou, P., Hailes, H. C., Hart, S. L., and Tabor, A. B. (2007) Targeting lipopolyplexes using bifunctional peptides incorporating hydrophobic spacer amino acids: synthesis, transfection and biophysical studies, *Bioconjugate. Chem.* (in press).
66. Irvine, S. A., Meng, Q. H., Afzal, F., Ho, J., Hailes, H. C., Tabor, A. B., McEwan, J. R., and Hart, S. L. (2007) Synthetic receptor targeted nanocomplexes for gene transfer to primary vascular cells and explant cultures of rabbit aorta, *Mol. Ther.* (in press).

BI701014Y